



# Initial Performance of the High-Pressure DT-Filling Portion of the Cryogenic Target Handling System

Cryogenic targets for the OMEGA laser are polymer shells of ~1-mm diameter and 1- to 5- $\mu\text{m}$  wall thickness that require internal  $\text{D}_2$  or DT solid layers of ~100- $\mu\text{m}$  thickness. Targets containing  $\text{D}_2$  may also be doped with gaseous  $\text{He}^3$  to aid in diagnosing the implosion using the charged-particle spectrometer. To achieve the required inner ice layer, shells are first permeated to a pressure of ~1000 atm at room temperature and then cooled to ~25°K. A slow, controlled pressure ramp to avoid buckling of the target and a slow, controlled temperature ramp to 25°K are required to successfully fill targets. The thinnest-walled shells, which are of the greatest interest, have buckling pressures  $\leq 0.1$  atm, which imposes a requirement of considerable precision in controlling the pressure differential across the shell wall during the pressurization and cooldown. LLE has constructed a system that successfully fills thick-walled targets and demonstrates the capabilities necessary to fill thin-walled targets.

## System Description

The pressurization portion of the Cryogenic Target Handling System achieves compression in two stages (as seen in Fig. 81.4): (1) by slowly heating the cryogenically concentrated  $\text{D}_2$  or DT and (2) by using a diaphragm compressor. The process begins with valves V1, V3, and V6 open, all other valves closed, and the targets evacuated. The condensation tube (volume 12.0  $\text{cm}^3$ ) is cooled to ~10°K, and the contents (~0.3 mole) of the  $\text{D}_2$  or DT vessel are condensed into it; then valves V4 and V5 are opened, providing a path for gas to reach the permeation cell, which contains four targets at room temperature. Next, valve V1 is closed and V2 is opened, allowing a small quantity of  $\text{He}^3$  to flow to the targets. A pressure of ~0.03 atm of  $\text{He}^3$  added at this point will produce a 5% concentration of  $\text{He}^3$  in the gaseous  $\text{D}_2$  in the center of a target at the triple point, 18.7°K. To start the first stage of compression, valve V3 is closed, and the condensation tube is slowly heated

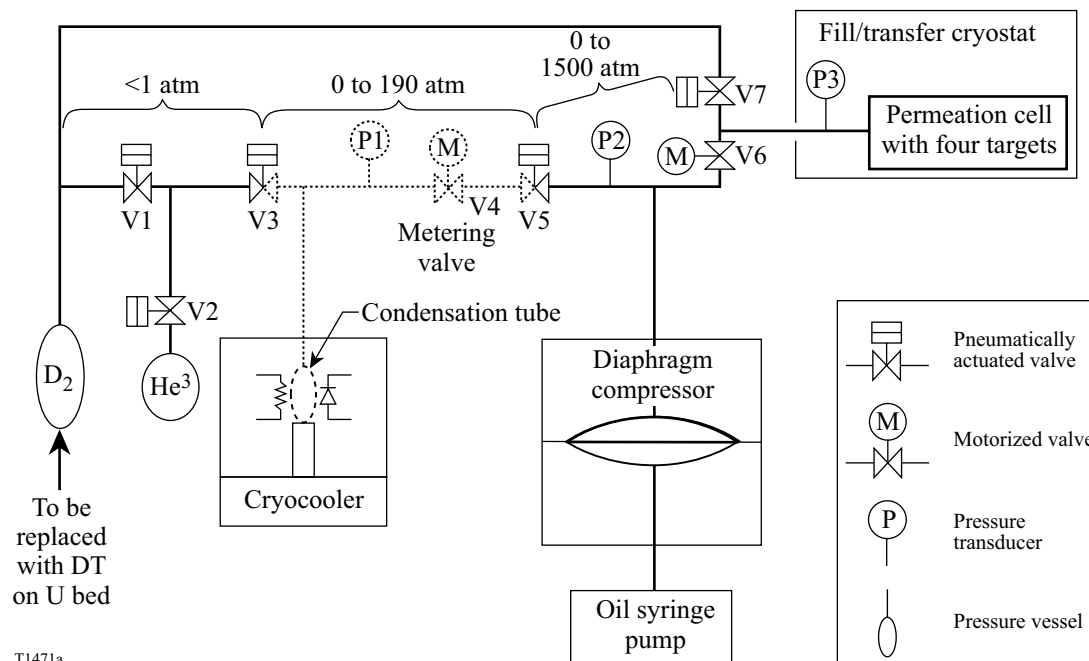


Figure 81.4

Abbreviated diagram of the pressurization portion of the system. The parts omitted include burst discs, limit switches, solenoid valves, and controllers.

until the pressure in the targets reaches ~150 atm (190 atm maximum). The second stage of compression is achieved by closing valve V5 and slowly driving the diaphragm compressor to the final pressure, typically 1000 atm (1500 atm maximum). This compressor has a flexible metal diaphragm with up to 30.9 cm<sup>3</sup> of gas on one side and hydraulic oil on the other. The oil is compressed by a syringe pump, which uses a piston (area = 1.60 cm<sup>2</sup>, stroke = 24.3 cm) linked by a gear train (126 turns/cm) to a stepper motor (1000 steps per turn). Although pressure transducers are located in both stages and on the permeation cell, system control depends primarily on the transducer P2—a highly accurate ( $\pm 0.14$  atm) Bourdon tube—in the second stage.

After the targets have reached the maximum pressure, they are slowly cooled to <25°K before the D<sub>2</sub> or DT external to the targets is pumped out of the permeation cell. For thick-walled targets, the cooling is done with valve V6 closed. Cooling must be done slowly enough that the cooled portion of the pressurization system remains isothermal, avoiding temperature gradients that could produce a pressure differential across the target wall, causing the target to burst or buckle. Thin-walled targets, because they are weaker, require an alternative cooling strategy:\* Valve V6 is left open, and the compression equipment is run in reverse to lower the pressure as the targets are cooled, keeping the measured external pressure very close to the calculated internal pressure. Once the targets are cooled to <25°K, the vapor pressure of D<sub>2</sub> or DT is <2 atm, and the gas external to the targets can be pumped out of the permeation cell without risk of bursting the targets. This pumping is done with valve V7 open; it continues (possibly for several hours) until the residual quantity of gas in the permeation cell will be manageable when the cell is unsealed and this residual gas is released into the cryostat.

\*If valve V6 could be located inside the cryostat and cooled along with the permeation cell so that all portions of the pressurized volume remained isothermal, the pressures internal and external to the target would be nearly equal throughout the cooling process. (A small excess pressure would still arise internal to the target because the thermal contraction of a polymer shell exceeds that of the metal permeation cell.) Such a cryogenically compatible valve is not available. If valve V6 is closed prior to the cooldown, the small volume in the room-temperature plumbing (~0.3 cm<sup>3</sup>, compared to 5.0 cm<sup>3</sup> of cooled volume) generates a pressure external to the target. This is because gas in the room-temperature portion is less dense than the cooled gas. The external pressure generated by this density difference is sufficient to cause thin-walled targets (wall thickness <5  $\mu$ m) to buckle. Success in cooling thin-walled targets with valve V6 open and the compression equipment running in reverse requires accurate determination of the target temperature and calculation of the corresponding internal pressure. Since thin-walled targets are much stronger against bursting than against buckling, the best strategy is to keep the external pressure slightly below the calculated internal pressure.

The system is controlled by a programmable logic controller (PLC), which is linked to a workstation with a graphical user interface (GUI). All valves and motors in the system are controlled by the PLC, which also monitors all pressures, temperatures, and the status of limit switches. The pressurization ramp is managed by control loops that include the high-accuracy pressure transducer, the condensation tube thermometer and heater, and the motor driving the oil syringe pump. These loops are executed and maintained by “C” programs residing in the PLC. The GUI software allows the user to monitor, log, and view data from the target-fill process in real-time. It also allows modification of the fill rate and parameters of the control loops. There are several hard-wired safeguards, such as limit switches that prevent excess piston travel in the syringe pump.

All system parts that will contain  $\geq 1$  atm of DT have been provided with secondary vacuum containment, with a glovebox providing tertiary containment. This secondary containment is divided into four chambers. Helium gas at ~0.5 atm will be circulated through three of these chambers with a circulation pump, while the fourth chamber is kept evacuated to insulate the condensation tube. The divisions of the secondary containment system are shown in Fig. 81.5. A modified ion gauge will detect tritium leakage with a resolution of ~10 mCi/m<sup>3</sup> at 1 atm and ~150 mCi/m<sup>3</sup> at <1 Torr. If a low-level tritium leak is detected, the tritium-contaminated helium will be pumped to the tritium recovery system, evacuating the contaminated chamber. High-level leakage will be routed with the circulation pump to a local uranium bed, which will absorb the DT. Volumes in the secondary containment chambers are sufficient to contain the entire DT inventory of 0.34 mole (10<sup>4</sup> Ci) below 1 atm at room temperature.

### Target Filling

Four targets are filled simultaneously. Each target is supported by three submicron strands of spider silk<sup>1</sup> as shown in Fig. 81.6. The spider silk is stretched across a beryllium wire frame, which is formed into a shape that avoids the OMEGA laser beams, and coated with a uniform, conformal layer of 0.1  $\mu$ m of parylene, which fastens the silk to the shell. The Be frame is attached to a boron fiber, which is in turn attached to an Al base. This mounting method is highly robust at cryogenic temperatures. The four targets are placed in a contoured copper holder, as shown in Fig. 81.6. The copper holder acts to improve the temperature uniformity inside the permeation cell and also provides a space filler to minimize the volume. With this holder inside the sealed permeation cell, the cooled volume is 5.0 cm<sup>3</sup>. Reducing the gap between the copper holder and the

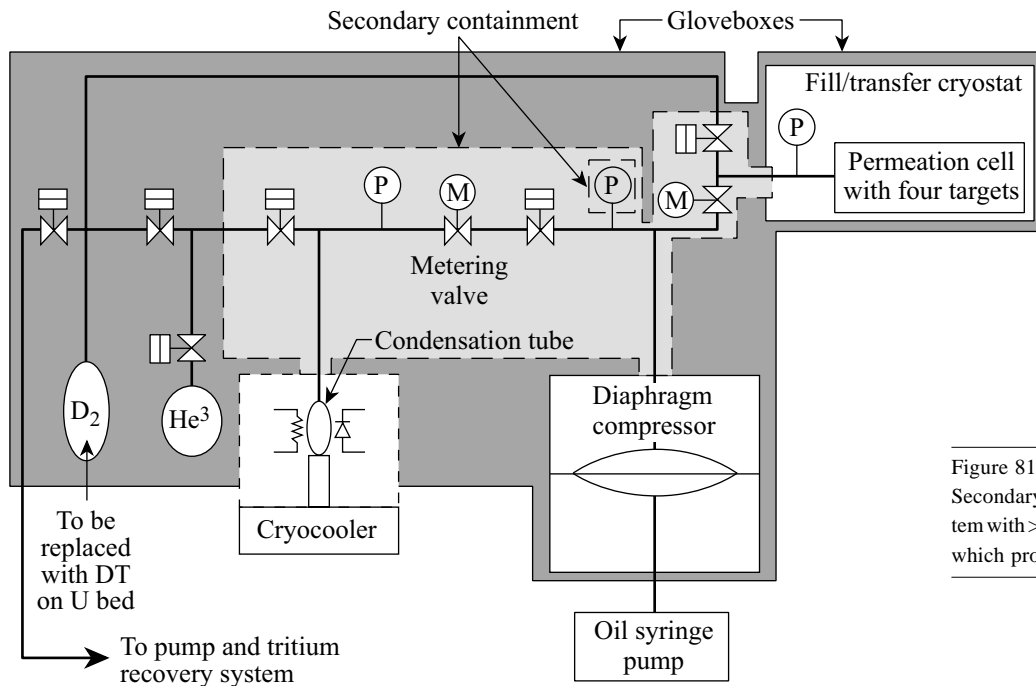
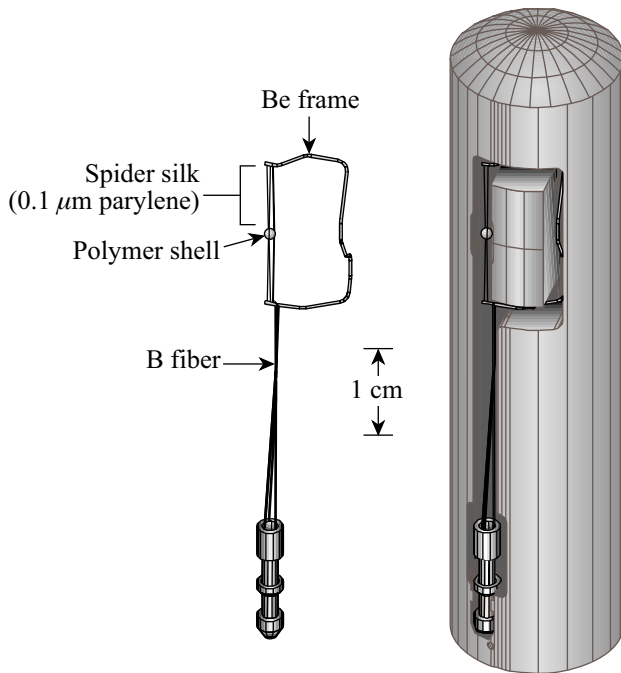


Figure 81.5  
Secondary containment for all parts of the system with >1 atm of DT, and the outer gloveboxes, which provide tertiary containment.

T1470

target support elements could reduce this volume, which would reduce the percentage of the DT inventory required to fill a set of targets (currently 82%). The tighter tolerances, however, would increase the difficulty of removing targets for transport, and a higher target attrition rate might be expected.



T1469

Figure 81.6  
Cryogenic target supported with spider silk, and a holder for four targets (only one of the four cavities is shown); also see p. 21, Fig. 81.21, this issue.

Filling thin-walled targets will take from 8 to 60 h, depending on the specifications of the targets. To fill them as quickly as possible, the pressure is increased at a uniform rate such that the external pressure exceeds the internal pressure by an amount  $\Delta P$ , which is less than the buckling pressure:<sup>2</sup>

$$\Delta P < \frac{8E}{[3(1-\mu^2)]^{1/2}} \left(\frac{w}{D}\right)^2, \quad (1)$$

where  $w$  = wall thickness,  $D$  = diameter,  $E$  = Young's modulus, and  $\mu$  = Poisson's ratio. For plasma polymer shells,<sup>3</sup> this formula was confirmed experimentally at LLE by pressurizing shells of various wall thicknesses in the 1- to 10- $\mu\text{m}$  range and measuring their buckling pressures. To compare the data to Eq. (1), the value of  $E$  used was 2.1 GPa, obtained by measuring the expansion of several plasma polymer shells due to internal pressure. The value of  $\mu$  used was 0.35 (the value for polystyrene, a glassy polymer with somewhat similar properties to plasma polymer). The permeation time constant for an ideal gas is given by

$$\tau = \frac{wD}{6pRT}, \quad (2)$$

where  $p$  = permeability,  $R$  = gas constant, and  $T$  = absolute temperature. Since  $D_2$  at high pressure is less dense than an ideal gas (62% of the ideal gas density for 1000 atm at 294°K), a larger time constant is expected at high pressure, suggesting that a cautious rate of pressure rise should be used. For a uniform rate of pressure rise, the pressure differential across the shell wall is proportional to the permeation time constant after a time  $t \gg \tau$ :

$$\Delta P = \tau \frac{dP}{dt}. \quad (3)$$

Combining Eqs. (1), (2), and (3), the maximum pressurization rate is proportional to wall thickness/(diameter)<sup>3</sup>:

$$\frac{dP}{dt} = \frac{\Delta P}{\tau} < \frac{48EpRT}{[3(1-\mu^2)]^{1/2}} \frac{w}{D^3}. \quad (4)$$

For a plasma polymer shell with  $w = 1 \mu\text{m}$  and  $D = 1 \text{ mm}$ , the buckling pressure is 0.1 atm,  $\tau = 10 \text{ s}$ , and filling to 1000 atm at room temperature requires more than 30 h. The filling time may be reduced by filling at an elevated temperature.

### System Performance

Several thick-walled targets have survived filling with  $D_2$  to a pressure of 1000 atm. In the first test, two mounted targets with 1-mm diameter and wall thicknesses of 10  $\mu\text{m}$  and 20  $\mu\text{m}$  were filled to 1000 atm over an 8-h period, left under pressure for 3 days, and then depressurized over an 8-h period. After removing the targets from the permeation cell, microscopic examination indicated no damage to the targets or the mounts. In the second test a similar pair of plasma polymer targets along with a polyimide target were pressurized and then slowly cooled to 20°K. The permeation cell was then unsealed, and the targets were viewed at 20°K through a fiber-optic borescope. The targets were seen to be intact. One of the targets was picked up with the robot arm and deposited on the tip of the moving cryostat, where the target was warmed. A sudden spike in pressure of the expected magnitude indicated that it had exploded, as expected, and that it had retained all the  $D_2$  from the filling process.

The performance of the two compression stages is studied by comparing experimental data to the  $D_2$  equation of state.

This comparison requires knowledge of the volume of each part of the system. The volume of each part is determined by connecting to a known volume and observing the pressure change when gas flows to or from the volume being measured. A 24-term equation developed by NIST<sup>4</sup> gives pressure as a function of density for  $D_2$  above the critical point (38.3°K), using terms up to the seventh power of density and sixth power of temperature. At temperatures below the critical point, saturated vapor pressures<sup>5</sup> are used. It is difficult to predict pressure and density accurately in the region of the critical point (and down to the point where the liquid phase begins), and it is planned to rely on data taken with the pressurization apparatus itself.

Performance of the condensation tube for pressure generation is shown in Fig. 81.7. The data are taken by condensing 0.123 moles of  $D_2$  (determined by measuring the change in pressure in the  $D_2$  supply reservoir and converting to moles with the equation of state), and then raising the temperature of the condensation tube slowly enough to assure isothermal conditions in the tube (the tube, made of stainless steel, is in good contact on all sides with copper of high thermal conductivity). The 0.123 moles are distributed between the 12.0-cm<sup>3</sup> cooled volume and the 5.32-cm<sup>3</sup> volume (tubing, burst disc, and valves) at room temperature. A good match is obtained between measured data points and the expected pressure, calculated with the NIST equation of state.

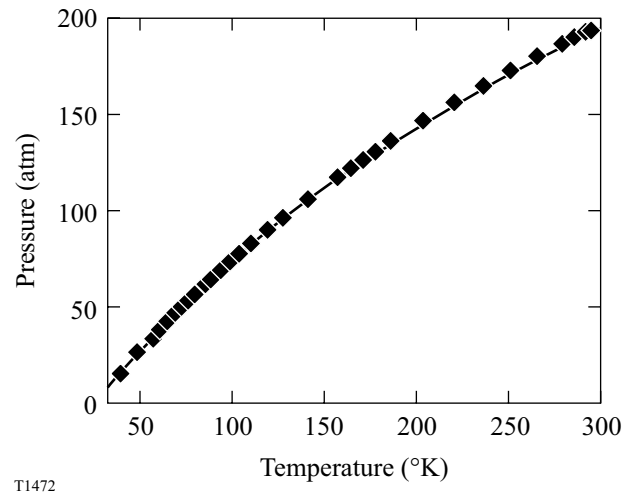


Figure 81.7

The pressure in the condensation tube (measured points) is accurately characterized by the  $D_2$  equation of state above 38°K (used to compute the solid line).

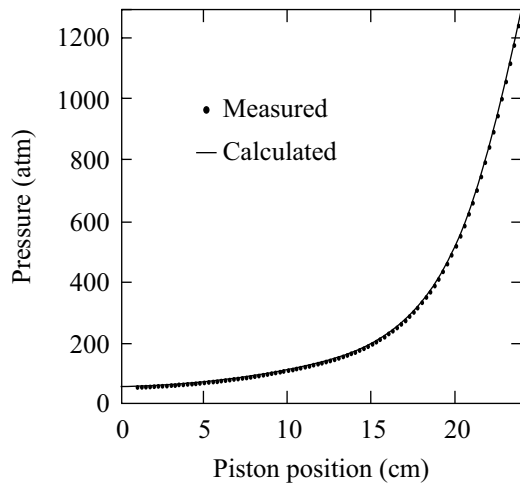
Analyzing the performance of the diaphragm compressor requires knowledge of the oil compressibility. The manufacturer of the compressor<sup>6</sup> supplies compressibility data for the oil,<sup>7</sup> which are fit by the equation

$$C(P) = b_1 (P/1 \text{ atm}) - b_2 (P/1 \text{ atm})^2, \quad (5)$$

where  $b_1 = 5.30 \times 10^{-5}$ ,  $b_2 = 6.4 \times 10^{-9}$ , and  $C(P)$  is defined as the fractional reduction in oil volume from its uncompressed value at pressure  $P$ . The expected pressure is obtained by first computing the  $D_2$  molar density,

$$\rho = \frac{M}{V_0 - [A \cdot z - V_{\text{oil}} \cdot C(P)]}, \quad (6)$$

where  $M$  is the number of moles,  $V_0$  is the initial volume,  $A$  is the area of the piston,  $z$  is the distance of piston travel, and  $V_{\text{oil}}$  is the uncompressed volume of oil. The pressure values entered in this equation are obtained by expressing the experimentally measured pressure data as a continuous function of  $z$ . The NIST equation of state is then used to convert density to pressure. Figure 81.8 shows good agreement between measured and calculated pressure. The fitting parameter adjusted to obtain agreement between measured and calculated pressures is  $V_{\text{oil}} = 113.5 \text{ cm}^3$ , which cannot easily be measured. In addition,  $b_2 = 4.2 \times 10^{-9}$  provided a much better fit at high pressures than the manufacturer's data. For this analysis, it has been assumed



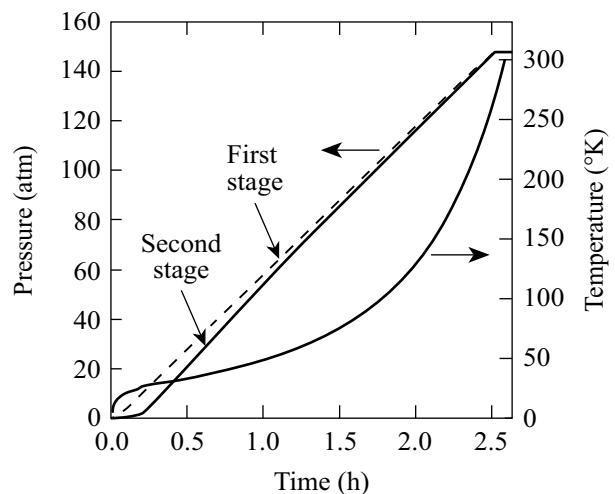
T1519

Figure 81.8

Pressure versus piston position is accurately characterized by the  $D_2$  equation of state and oil compressibility data. Error bars for the measured points are too small to see. The maximum difference between measured and computed pressures is 8 atm for the whole data set, 2 atm at pressures <500 atm, and 0.1 atm at pressures <160 atm.

that the oil pressure and gas pressure are the same, and that the extra component of oil pressure required to deform the diaphragm is negligible.

To pressurize targets, a temperature versus time profile is calculated for the condensation tube, using vapor pressure data, and the equation of state. This calculated profile is used to program a temperature controller, which uses a PID loop to control the temperature. An example of a successful temperature profile and the resulting uniform rate of pressure rise is shown in Fig. 81.9. The difference in pressure between the first and second stages is due to the metering valve, fully open in this case. The ramp that was obtained would be suitable for a shell with a 3- $\mu\text{m}$ -thick wall and a 1-mm diameter, but the method should work equally well to generate a pressure ramp suitable for a shell with a 1- $\mu\text{m}$  wall. Hidden in these data are small departures from a constant rate of pressure rise, which should be correctable by adjusting the temperature profile with measured data near the critical point. This procedure's success in generating a constant rate of pressure rise offers an opportunity to eliminate the metering valve. There is strong incentive to eliminate this valve because of stem-seal leakage. Leakage through this valve stem was detected by pressurizing the system with He and was not eliminated by replacing the O-ring. The stem is sealed by a single O-ring, which appears not to be sufficiently constrained. Even if constraints on the O-ring were improved, leakage would be expected when the valve stem is moved.

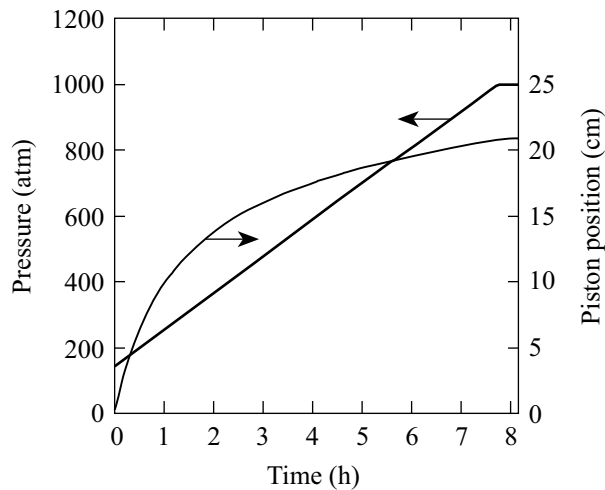


T1488

Figure 81.9

A uniform rate of pressure rise is produced by applying a calculated temperature profile to the condensation tube.

To generate the high-pressure portion of the pressure ramp, a valve is closed to isolate the diaphragm compressor from the condensation tube. The piston of the syringe pump is then given an initial velocity, and a simple algorithm is applied to the resulting rate of pressure rise to adjust the piston velocity to match the desired rate of pressure rise. The result is shown in Fig. 81.10, which shows a pressure ramp suitable for a shell with a 5- $\mu\text{m}$  wall thickness. Upon magnification of the pressure versus time data in Fig. 81.10, the pressure is found to be increasing smoothly at all times, with small variations in slope due to the control algorithm. No obstacle is found to the use of a much slower rate of pressure rise, which would be suitable for filling shells with 1- $\mu\text{m}$  wall thickness.



T1474

Figure 81.10

A constant rate of pressure rise is produced by controlling the piston position with a simple algorithm.

The pressurization system has proven robust, with all indications that it will be able to fill shells with the thinnest walls. Three additional observations contribute to this conclusion. The smallest motion increment of the motor driving the oil syringe pump corresponds to 0.002 atm at a pressure of 1000 atm, and less at lower pressures, much less than the 0.1-atm buckling pressure of shells with 1- $\mu\text{m}$  wall thickness.

When the motor direction is reversed, as will be necessary when cooling thin-walled shells, there is one turn of backlash in the mechanical system, but no observable pressure drop that could threaten shell survival. Finally, it appears that the low rate of temperature rise required for the condensation tube ( $\sim 0.1^\circ\text{K}/\text{min}$  at  $40^\circ\text{K}$ ) is achievable by applying a slowly increasing power level  $\sim 12$  W. To demonstrate the capacity to fill thin-walled shells, a series of increasingly slower pressure ramps will be used to fill successively thinner walled shells, followed by depressurization ramps and examination of the shells. The final and most difficult step will be to again fill such targets and reduce the external pressure while cooling the targets by running the pressurization apparatus in reverse.

#### ACKNOWLEDGMENT

The pressurization portion of the CTHS is based on a conceptual design by General Atomics. The use of spider silk to support targets was pioneered by S. G. Noyes of LLE, who also developed the present attachment method. This work was supported by the U.S. Department of Energy Office of Inertial Confinement Fusion under Cooperative Agreement No. DE-FC03-92SF19460, the University of Rochester, and the New York State Energy Research and Development Authority. The support of DOE does not constitute an endorsement by DOE of the views expressed in this article.

#### REFERENCES

1. B. A. Brinker, J. M. Cavese, J. R. Miller, S. G. Noyes, S. Sheble, and L. T. Whitaker, *J. Vac. Sci. Technol. A* **1**, 941 (1983).
2. W. C. Young, in *Roark's Formulas for Stress & Strain*, 6th ed. (McGraw-Hill, New York, 1989), p. 691.
3. S. A. Letts, D. W. Myers, and L. A. Witt, *J. Vac. Sci. Technol.* **19**, 739 (1981); S. A. Letts *et al.*, *Fusion Technol.* **28**, 1797 (1995); B. W. McQuillan *et al.*, *Fusion Technol.* **31**, 381 (1997).
4. R. Prydz, K. D. Timmerhaus, and R. B. Stewart, in *Advances in Cryogenic Engineering*, edited by K. D. Timmerhaus (Plenum Press, New York, 1968), Vol. 13, pp. 384–396.
5. P. C. Souers, *Hydrogen Properties for Fusion Energy* (University of California Press, Berkeley, 1986), p. 52.
6. Fluitron, Inc., Ivyland, PA.
7. This type of oil is "Tellus 10" made by Shell Oil Company, Houston, TX.

